Detailed Numerical Analysis of X-ray Radiography in Sprays

Mark A. Linne*
Combustion Engine Research Center, Department of Applied Mechanics
Chalmers University, Gothenburg, Sweden
mark.linne@chalmers.se

Abstract

Recent studies of spray-related flowfields using synchrotron-based x-ray radiography at the Advanced Photon Source (APS), Argonne National Lab, have produced useful results related to fuel mass fraction. For some, however, it is not clear whether or not the technique can observe intact structures (e.g. a liquid core) inside a spray or not. Here we simulate x-ray radiography using a code that solves the full diffraction problem (Maxwell's equations subject to assumptions that apply in this case) to model accurately several common spray architectures found in the literature. One important finding is that radiography detects the total mass along a line of sight, including intact liquid, drops and in some cases vapor and gas. Under appropriate conditions, radiography reveals liquid mass fraction which is related to the spray breakup rate and gas entrainment; both critical for understanding of sprays. The single point system used at the APS provides a spatially and temporally resolved (but averaged over a number of injections) determination of liquid fuel mass fraction. The potential for confusion between local signal reduction by diffraction and local signal reduction by absorption is also discussed. The issue is not unusual in such circumstances. This potential background problem can be avoided by careful arrangement of the experiment and it is clear that it does not affect the results produced by the Advanced Photon Source.

Introduction

Figure 1 depicts a transparent diesel fuel injector tip that was used to observe cavitation inside one hole of the tip, using microscopic shadowgraphy [1]. One can see a small stream of cavitation bubbles inside the hole and leading to the nozzle exit. Note what happens once the jet exits the hole. The fact that the spray (consisting of droplets on the order of 5 – 10 μm diameter) does not instantaneously spread indicates that many of the larger liquid structures visible inside the hole must still exist outside of the hole, as intact liquid structures (perhaps a liquid core or perhaps a collection of more distributed liquid structures) undergoing primary breakup within the droplet cloud. These structures were hidden from view by the camera, however, because the droplet cloud was very dense and the density of this region has presented a significant measurement challenge to simple, classical optical techniques.

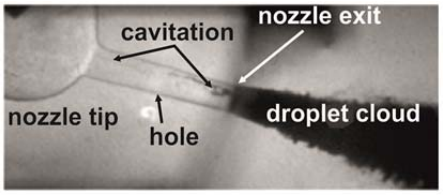

Figure 1 Microscope shadowgram of flow inside an optical diesel nozzle tip (reproduced with permission [1]*).*

Within the last decade, two very different approaches to this challenge have been proposed, developed, and discussed. One of them is ballistic imaging (BI [2]); a laser-based (optical) technique. The stated goal of BI is to develop better understanding of primary breakup mechanics by extracting images of intact liquid structures that are buried within the droplet cloud in the spray formation region. BI takes advantage of the fact that a very small amount of light passing through a dense spray is not deviated by the droplets; it passes straight through the cloud. This small amount of light is refracted by the larger liquid structures, however, just as it would be in the absence of the drops. This high quality imaging light (often termed "ballistic") can be used to create a shadowgram of the larger, intact liquid features inside the cloud. BI thus aims to reject almost all of the light headed towards the camera because it is corrupted by multiple scattering off-axis. Note that the signatures of corrupted light rely upon the fact that it scatters at large angles. BI shadowgrams have limited dynamic range compared to shadowgrams from open flows (e.g. without drops) owing to the small amount of light available in a single-shot image format, but they do reveal the liquid/gas interface of intact liquid structures (when they exist) with good spatial resolution. BI has been applied to a number of sprays and in a double-image format it has been used with image correlation techniques to generate images of the velocity of the liquid/gas interface and of primary drops that are large enough to be imaged by the technique [3].

The second approach is to use x-ray radiation. A research group at the Advanced Photon Source (APS) at Argonne National Laboratory has applied their high brightness synchrotron source to spray studies [4-12]. The stated goals of the x-ray program are to provide "quantitative data regarding fuel distribution" [11] (e.g. fuel mass) and to "visualize the near-nozzle morphology (~ 6 mm) and to better understand the primary breakup

* Corresponding author: mark.linne@chalmers.se

process" [12]. The APS group has reported extensively on x-ray phase contrast imaging in various kinds of sprays. That work is discussed in a companion article to this one [13].

The APS group has also reported x-ray radiography in various kinds of sprays. Radiography is line-of-sight absorption imaging, wherein an x-ray beam passes through the spray (see Figure 2), portions are absorbed by the liquid, and the resulting beam energy is measured or imaged. Absorption is controlled by the Beer-Lambert law (Equation (1)); where τ is the transmission through an absorber ($\tau \leq 100\%$), I_ℓ is the irradiance (W/m^2) if the x-ray beam after passing a distance ℓ (cm) through the spray, and I_o is the irradiance before entering the spray. The x-ray community writes this expression using a mass-based absorption coefficient μ_m (cm^{-1}).

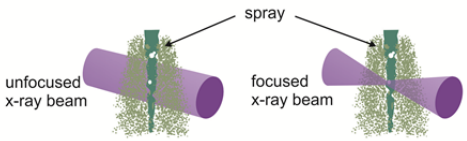

a. b.

Figure 2. Example x-ray radiography geometries.

$$\tau = \frac{I_\ell}{I_\circ} = e^{-\mu_m \ell} \quad (1)$$

The initial radiography results were presented in a number of articles [4-7], including an article featuring tomographic reconstruction, and those articles were followed by a review paper [14]. As one example, Figure 3 provides a well-known radiography image of a spray produced by a single hole diesel injector issuing into SF_6 at 1 bar [4] (recent results include similar images of such sprays, e.g. [11]). In the first set of experimental campaigns, the fuel spray was illuminated with a synchrotron x-ray beam from the APS, with photon energies on the order of 5.5 to 7 keV (wavelengths on the order of 0.2 nm)[1] in a line-of-sight configuration (Fig. 2a). Liquid fuel mass locations were determined by the level of x-ray beam attenuation as it crossed the spray, and it was detected by a two-dimensional x-ray pixel array detector (PAD) [6]. Insufficient x-ray absorption by the fuel at this photon energy (wavelength) required the use of a contrast agent (a Cerium-based additive) to increase absorption of the x-ray beam, while low signal-to-noise ratios (SNR) required averaging over several injection cycles. The image of one spray was thus developed over a number of injection events. The x-ray absorption images in references [4-6] had relatively limited spatial resolution (roughly 5 - 10 mm in the axial direction). The overall images are constructed of a number of individual measurement points pasted together.

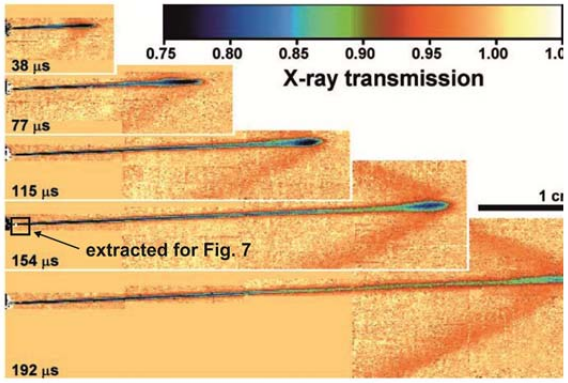

Figure 3. Radiography image of a Diesel spray (reproduced with permission [4]).

There is a significant advantage to x-ray radiography; it can be a quantitative, line-of-sight absorption technique following the Beer-Lambert law. Moreover, at these wavelengths the drops do not scatter significantly [13]. If one measures the beam extinction (e.g. does a calibration measurement of μ_m caused by absorption in a known mass of fuel with known ℓ) one can have an absolute determination of fuel mass. The images can thus be directly related to fuel mass fraction [15] and that term is critical for understanding of fuel sprays. Techniques for calibration and detection of absolute mass are discussed in detail by Linne [16].

Because x-ray radiography is a promising way to determine total fuel mass as a function of position, it continues to be applied and improved at the APS [8-11, 17-19]. Kastengren et al. [19] describe the recent development of an APS beamline (7-BM) dedicated to spray radiography. This beamline covers the photon energy range from 5 to 12 keV with central energy of 8 keV, and a photon flux up to 30 x 10^{11} photons/(sec. mm^2). This represents significantly more flux than in the past and that can provide better SNR. The beamline hosts two experimental hutches for spray radiography. In a following paper [11] the group described detailed radiography measurements in a single hole Diesel spray at 8 keV during multiple injections. The high x-ray flux of this new beamline also allows them to use windows that hold off 20 bar air pressure in the spray chamber, which is an important improvement. In reference [11], the beam was focused to a spot size of 8 µm x 10 µm (Figure 2b.), passed through the spray, and the beam was then directed to a single avalanche photodiode detector. This new strategy is intended to achieve good spatial resolution while raster scanning the spray over multiple measurements ("several thousand injection events"). Each measurement occurs over time scales that are short with respect to fluid times, so they are time resolved as well. The measurements are thus spatially and temporally resolved but averaged over many cycles. The Ce-based contrast agent is not always used now. The authors coupled

[1] Note that in the x-ray regime we use photon energy ($E = hc/\lambda$) to describe wavelength of light; where h is Planck's constant, c is the speed of light in vacuum and λ is the wavelength.

these spray measurements to x-ray phase contrast images of needle motion inside the injector at much higher photon energy (in a different beamline).

There are analogies and differences between optical and x-ray absorption, just as there are analogies and differences between the optical and x-ray diffraction problems. Optical spectroscopy involves interactions between light and the quantum states of an atom or molecule [20]; controlled roughly by transitions between two valence electronic quantum states in the UV, and by transitions between two rotational-vibrational quantum states the infrared. In contrast, x-ray absorption targets core shell electrons (outside of the VUV) in atoms that are either isolated or bound to other atoms in a molecule. The absorption response of the atom is to eject the electron that was targeted, from a core level to a continuum (free electron) or conduction level. These interactions are termed 'k-edge' when the targeted electron is in an *s* atomic orbital, 'l-edge' from a *p* orbital, and 'm-edge' from a *d* orbital. The k-edges involve high photon energy, l-edges somewhat smaller, and m-edges even smaller. In Figure 4, for example, the Pb spectrum shows an m-edge at low energy, three l-edges at intermediate energy and a k-edge at high energy. Conversely, the O-atom has a k-edge at 537 eV; below the range of this plot and so no O-atom edges are in evidence. Finally, note that μ_m has a baseline trend that falls with E, which is why hard x-rays can be transmitted through materials when soft x-rays cannot.

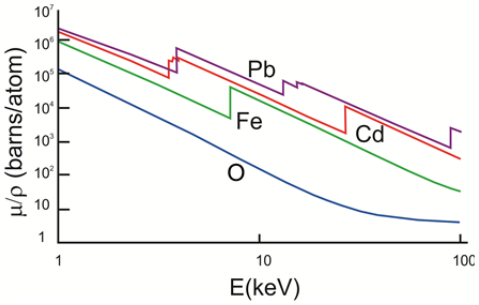

Figure 4. Absorption spectra for several atomic elements. The vertical axis is a normalized absorption coefficient (same as a cross section per atom).

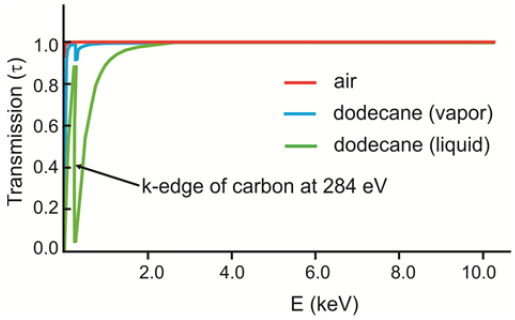

Figure 5. X-ray transmission.

For measurements in sprays, the goal is to observe absorption in the liquid fuel under conditions where the surrounding gas does not absorb. Figure 5 contains transmission spectra (τ vs. E) for 100 μm absorption path lengths (small) for dodecane (liquid and pure vapor) and air, from 15 eV to 10 keV, generated using the online database at NIST. The red curve shows that air does not absorb strongly over this range. At the left hand side of the plot, the green curve for liquid dodecane starts to rise up as μ_m decreases (following the baseline trend mentioned above) until the photon energy hits the carbon k-edge, at which point the transmission drops precipitously owing to absorption. Following that interaction, transmission rises as μ_m decreases again. Dodecane in the vapor phase (blue curve) absorbs much less across this entire region, but only because μ_m is proportional to density and the Lambert-Beer law is exponential in μ_m. The fuel vapor does have appreciable absorption right at the k-edge but otherwise it is roughly as transmissive as air (shown in red). Absorption in moderate sized features is thus very small in all three cases, and absorption in the gas phase is not very different from the liquid phase when E > 4 keV.

Methods

The simulations presented in reference [13] were performed using a commercially available code named General Laser Analysis and Design (GLAD). The same code is used here. The code provides solutions to the full diffraction problem described by Lawrence [21]. The method is discussed in more detail in Linne [22].

The simulation propagates x-ray radiation at 8 keV photon energy through a sample (single drop or collection of drops) followed by propagation through air out to D = 70 cm (a standard distance discussed in [22]). The APS has performed radiography both in an imaging format and at single point using a focused beam. Here we simulate the imaging format (Figure 2a.), which supplies the necessary information for both setups. A flat-topped, super-Gaussian x-ray beam profile is assumed (the beam diameter is adjusted to accommodate each problem). At 8 keV, the real index of refraction for fuel is (1-2.6 x 10^{-6}) and for air it is (1-1.5 x 10^{-9}).

To simulate absorption, it is possible to extract known values for μ_m from an x-ray database and use them in GLAD. As mentioned, until recently APS has exercised the freedom to choose any transmission level they wanted based upon how much Ce-based additive they used. Here, we just insert a range of values for μ_m to cover the possible ranges one might encounter in transmission. Simulations for a beam that propagated through single drops of diameter d = 100, 30, and 7 μm have been performed. Each drop size was evaluated using four different values for μ_m, starting with a value that is nearly 100% transmissive and going down to near zero transmission. Because three different drop diameters are evaluated, each drop will have a different level of transmission on centerline for the same value of μ_m. This may seem like a poor choice of variables, but each drop has varying ℓ anyway; ℓ = 0 at the edge and it increases to ℓ = d at the center. Furthermore, if we were to match transmission τ

for the three drop centerlines, then when we analyze groups of drops it would not be clear how to set μ_m. For these reasons, it seems best to choose fixed values for μ_m of 8, 150, 900 and 1600 cm^{-1} and proceed.

Results and Discussion

Figure 6 presents several images for the droplet size range of interest using a super-Gaussian x-ray beam profile with a width of 200 μm for the 100 μm drop and a super-Gaussian width of 100 μm for the 30 μm and 7 μm drops (note this means there is a scale change in Figure 6 from the first column to the next two). The drop diameter 100 μm was evaluated here (instead of the 80 μm used in reference [13]) because 100 μm is closer to the size of a feature that could potentially be buried inside a spray studied by radiography at the APS. The "5-beam solution" (a broader bandwidth approach) discussed in reference [13] was used here. The first column in Figure 6 contains cross-sections of the 100 μm drop as one would image it at a position 70 cm from the drop, for the values of μ_m listed above. The second column contains images for the 30 μm drop and the third contains data for the 7 μm drop. The first row represents simulations for μ_m = 8.0. The results look nearly identical to the phase contrast images (with τ = 100%) for similar drop sizes presented in [13]. Upon inspection, it is clear that diffraction remains an important contributor to the images in Figure 6.

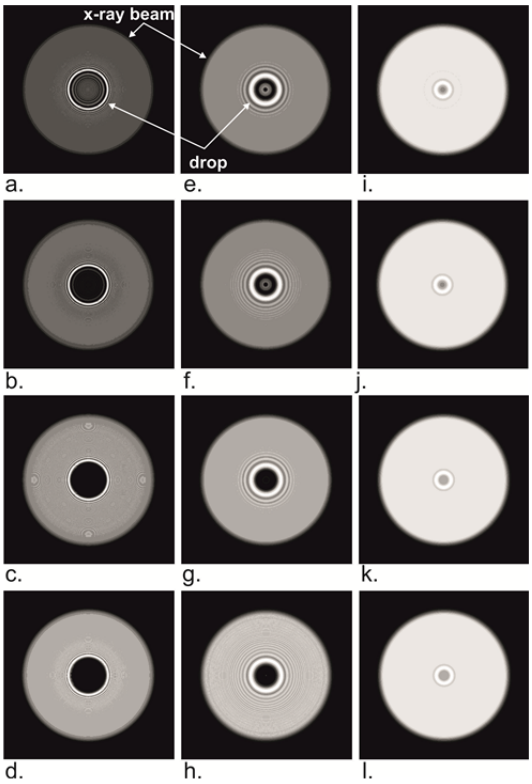

Figure 6. X-ray absorption in 100, 30 and 7 μm drops (see text).

In Figure 6a. one can see a thin, large diameter light band outside a thin, large diameter dark band, both characteristic of diffraction. The total energy in a beam after an ideal (elastic) diffraction process is the same as the energy in the beam just before diffraction. The pattern simply rearranges the energy into lighter and darker bands. There are many other, finer structures (bands and finer patterns) in the image, but as explained in detail in reference [22] those are the result of the relatively narrow bandwidth of this simulation together with the fact that we have not simulated the finite spatial resolution of the actual instrument. Phase contrast images taken by a broad-band, incoherent x-ray beam include the large diameter and more pronounced dark and light bands, but not the other finer structure. It is the large structure that is important here.

As center-line transmission is reduced to 23% for the 100 μm drop (Figure 6b.), the center of the drop is dark but the edges are fairly light. At μ_m = 900 cm^{-1} (e.g. τ = 0.0% on centerline, Figure 6c.), the drop has gone black but the light diffraction ring remains. Once the drop has reached 0% transmission all of the interior information beyond that value of μ_m is lost. If this were an intact liquid structure inside a spray it would not matter that it had gone black unless there happened to be a bubble inside it. Perhaps the most useful outcome of radiography imaging is determination of the fuel mass fraction and so the presence of a bubble would be useful information.

A drop size of 30 μm was evaluated because that is a commonly encountered average drop size in other types of sprays. Lin et al. [23], for example, have studied an effervescent spray whose drop size distribution includes 30 μm drops. For a 30 μm drop the dark band is a larger fraction of the total image (Figure 6e., remembering the scale change). Again, as the level of absorption increases the center goes completely dark.

The 7 μm drops are in the size range one typically encounters in a highly atomizing Diesel spray. As in reference [13], the diffraction pattern for such a small drop is a gray pixel. As absorption is increased, the gray pixel changes in a less obvious way. Very little energy has been lost from a 100 μm beam when passing around a small drop that allows 33% transmission on centerline.

The dark diffraction bands under transmissive values of μ_m (the top row of Figure 6) could easily be confused with absorption. This is a classic problem when phase contrast phenomena (often unavoidable, as here) and absorption are combined. The work performed by APS has not been strongly affected by this problem, however, for a number of reasons. Most importantly, the focused beam format means that the entire beam is sampled at the detector. As mentioned above, if one were to surface-integrate the energy in an elastic diffraction pattern the original total energy that entered the system would be recovered. By detecting the total energy of the beam, the APS acquires this entire signal and avoids confusion between dark and light diffraction regions. The loss of energy caused by absorption, however, can still be registered with high precision.

For completeness, the question of imaging formats should also be addressed. First, the combination of a 100 - 150 μm drop (similar in size to potential intact interior structures) with 7 μm drops is most closely related to the

ongoing radiography work at the APS. The contribution of the dark diffraction band decreases as the drop size increases, so the larger sizes are less susceptible to this systematic offset, and small drops simply do not suffer as much from this diffraction darkening offset to begin with. Finally, any kind of averaging (surface averaging by spatial resolution, averaging over multiple shots etc.) will quickly remove residual diffraction darkening effects.

Figure 3 contains a representative set of images acquired by x-ray radiography in a spray produced by a single-hole Diesel injector. This image was generated using the PAD detector, but it is similar to more recent raster scanned single-point measurements at higher spatial resolution [11, 19]. A related article [24] stated that "The x-ray technique also provides the ability to measure the ... breadth of the fuel distribution very near the nozzle, without obfuscation by the surrounding droplets." The statement about avoiding obfuscation by droplets (and similar statements) raises the question of whether or not drops contribute to the radiography images. The answer affects how one should interpret the data. Note the bulb of highly absorbing material at the very tip of the spray in Figure 3. One would not expect to see intact liquid structures located so many nozzle diameters away from the tip of a Diesel injector, especially because the liquid appears to have diminished somewhat with distance only to reappear at the tip. The tip, however, is where a stagnation zone would cause the leading drops to slow down and the oncoming drops would then collide with them. That would build up liquid mass in the form of larger drops, not as an intact liquid structure that had survived from the nozzle. An explanation based on drops could easily explain the images. We hypothesize, therefore, that x-ray radiography as performed in [4] detects any form of liquid fuel, including droplets, and that these drop signatures will never leave the x-ray beam (consistent with [13]).

This hypothesis was tested by modifying a case presented in [13]. This model uses very many randomly located 7 μm drops to simulate a spray, and the "1-beam solution" discussed in reference [13] was used to provide memory savings. As before, we include a 150 μm drop (called the 'core drop') that is located behind a simulated drop cloud. The core drop is meant to simulate the contribution of an intact liquid structure. Following that, square planes of drops (150 μm per side) were used, and 50 drops were randomly located in each plane (in x and y). Each of the planes was then spaced 10 μm away from the foregoing plane (along z). A 300 μm super-Gaussian x-ray beam was propagated through and around 48 planes with fifty drops each (2,400 drops total). There were about 8 - 12 drops standing between the edge of the core drop and the detector. The spatial resolution of the experimental imaging system plays a major role. The early image in Figure 3 had a spatial resolution on the order of mm, but Kastengren et al. [11] now report resolution between 8 and 10 μm. Our interest lies in the optimized system so here we simulate a resolution of 8 μm. To do that we apply a Gaussian filter with FWHM of 8 μm to simulated images in this section.

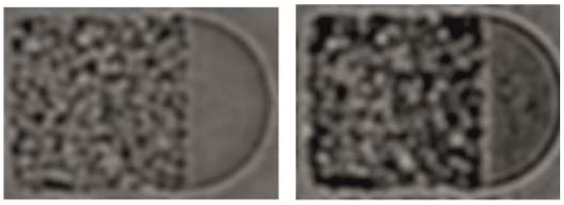

Figure 7. Absorption in a 150 μm large core drop and a fog of 7 μm drops.

Figure 7 contains two fairly transmissive images from the Diesel simulation. They are cropped to reveal just the spray-related parts of the images. To the right in each image one can see a portion of the core drop where there are no smaller drops. To the left one can see the contribution of the drop cloud (150 μm x 150 μm). Figure 7a. is a reproduction of the diffraction solution from [13] (with μ_m = 0.0 cm^{-1}, τ = 100%), but with an 8 μm FWHM Gaussian filter this time. Figure 7b. depicts the same problem but with μ_m = 8.0 cm^{-1} and τ = 99% on centerline for a single 7 μm drop, but in this case there can be as many as 10 drops along the line of sight (τ = 90% on centerline) and of course the extinction caused by the core drop will contribute to loss even more.

A first step is to compare Figure 7 to the images in Figure 3. To do this, the square that is called out in Figure 3 has been extracted, expanded, and reproduced in Figure 8. The small white rectangle in Figure 8 depicts the area of analysis as shown in Figure 7 (but rotated 90º). The experimental image has lower resolution than the simulation. One should think of the simulations as high resolution analyses of what lies behind the images from [4]. As mentioned, the images in [11] look somewhat similar to those in [4]; the same comments apply.


Figure 8. Square from Fig. 3, white area corresponds to size of images in Fig. 7 (rotated 90º).

Figure 7 makes one thing clear; radiography detects both intact liquid and drops. As in reference [13], simulations were extended out to a distance of 5 m from the spray and the drop signatures remained in the beam. Any x-ray radiogram acquired as in [4] will contain signatures from both intact liquid and drops; the hypothesis is correct. Once established, however, this fact helps one interpret the images. They represent total liquid mass, which is related to total liquid mass fraction. More recently the APS has reported mass per unit image area which simplifies some of the calibration discussion of reference [16]. It is also important to emphasize that we have analyzed just liquid absorption; assuming that vapor and gas absorption are negligible. Normally, the APS studies sprays that do not vaporize, so fuel vapor has not been an issue. Gas absorption is negligible if liquid absorp-

tion dominates (e.g. if contrast enhancing agents are used). Especially at higher gas density and when contrast agents are not used, however, gas absorption can contribute (see e.g. the relative transmission levels for gas and liquid in Figure 4). In almost every case, however, gas absorption can be considered spatially uniform in comparison to the liquid fuel.

Note also that the transmissive image (7a.) has dark features caused by diffraction. As discussed above they could be confused with absorption in an imaging format. Reference [13] demonstrates, for example, that drop cloud edges can produce somewhat darker filament features; simply via diffraction. One can see that phenomenon in the edges of the rectangular cloud in Figure 7. As mentioned already, however, purely elastic diffraction does not actually reduce the total energy in the beam. If one averages over larger areas than those shown in Figure 7, this systematic offset can be mitigated. Consider again the small rectangle in Figure 8. It is a very small fraction of the overall image. Figure 3 is an image with pixelation indicating spatial averaging over areas much larger than Figure 7, avoiding systematic intensity offset caused by diffraction.

Figure 9 contains similar images for μ_m = 150 cm^{-1} (Fig. 9a.), μ_m = 900 cm^{-1} (Fig. 9b.) and μ_m = 1600 cm^{-1} (Fig. 9c.). Figure 9a. is absorbing, and diffraction is barely in evidence. Again, the fact that the core drop is thicker and thus absorbs more radiation makes it possible to detect its presence behind the drop cloud. One can also see remaining evidence of the cloud in front of the core drop, emphasizing the fact that a line of sight technique like this will register fuel mass fraction as a composite signal averaged across both drops and an intact liquid structure if it is buried within the drops.

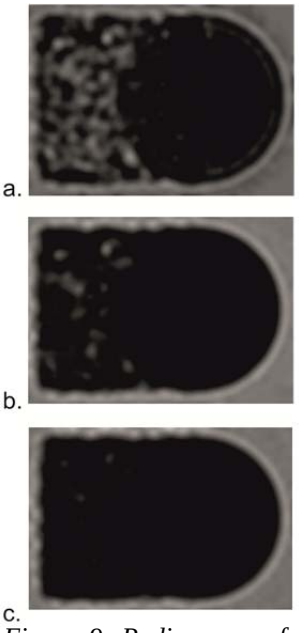

Figure 9. Radiograms of 7 μm drops in front of a core drop, for various values of μ_m.

Comparing Figure 7a. to Figure 7b. and to Figure 9a., one can see that moderately absorbing conditions reveal the liquid core behind the drop field better than Figure 7a. That happens because Figures 7b. and 9a. represent a fairly transmissive case, and so the evidence for the larger and less transmissive structure behind the more transmissive drop cloud can be detected. The APS has recently begun to perform tomographic imaging (time-averaged) [25] on Diesel sprays without contrast enhancing agents (a fairly transmissive case). Most recently they have discovered that the tomographic images have a structure that is best described by a narrow, peaked Gaussian spatial distribution in the center of the image and then a wide Gaussian distribution to describe the rest of the spray. One explanation could be that they are detecting a much denser cloud of drops or intact liquid structures (much stronger absorption signal) inside a more diffuse cloud of drops (somewhat reduced signal). This possibility is well worth further investigation. To image (within the spatial resolution of the system) in 3-D an intact liquid structure or dense drop formation together with the spatial distribution of a less dense drop cloud at the same time (if that is what exists) would be genuinely groundbreaking.

Figure 9b. is now missing most of the diffraction signature but the information in the center of the core drop is also lost. Figure 9c. is even more strongly absorbing. The information contained in the core drop has disappeared and most of the information in the drop cloud has also been lost. That case is clearly too highly absorbing and should be avoided.

One small issue with single-point detection is depicted in Figure 2b. The sample system looks like two matched cones touching at the tips. The beam has larger diameter before and after the focal point, so the contributions from the edges of the spray (all drops) are not acquired with the same beam diameter as at the core. This effect grows as the sample point is moved down the spray because the spray expands with distance. Kastengren et al. [11] don't provide details about the beam so it is not possible to estimate how much this change in beam size through the spray affects image results.

Next we model a field of 30 μm fuel drops. This problem is related to the flow produced by a jet in cross flow, for example, and it follows the pattern of analysis for the effervescent spray discussed in reference [13]. Indeed, Lin et al. [26] very recently announced radiography measurements in the same spray. As before, we locate a 150 μm core drop behind the drop cloud. This time the cloud is simulated as several 4-drop arrays with spacing of 60 μm (center to center, see reference [13] for details). Figure 10 contains 5-beam simulations using a 300 μm super-Gaussian beam traversing first through the core drop followed by one hundred 4-drop arrays, with eight drops at most between the edge of the core drop and the detector. Spatial resolution of 8 μm was simulated again via a Gaussian filter. Figure 10a. is a reproduction of the diffraction solution from [13] (with μ_m = 0.0 cm^{-1}, τ = 100%), but with an 8 μm FWHM Gaussian filter this time. Figure 10b. depicts the same problem but with μ_m = 8.0 cm^{-1}. Figure 10c. is for μ_m = 150 cm^{-1}, while Figure 10d. is for the case of μ_m = 900 cm^{-1}.

The images in Figure 10 demonstrate the issue identified before; diffraction darkening could be confused with absorption in an imaging format. In this case the diffraction patterns are large; the drop size is now a significant fraction of the jet size, and the spatial averaging required to mitigate the problem would make it impossible to resolve any jet structure. With 30 μm or larger drops it seems impossible to acquire high fidelity radiography images, but raster scanned single point mass measurements (multiple shots) would produce reliable results. That approach was adapted by Lin et al. [26] to provide reliable results.

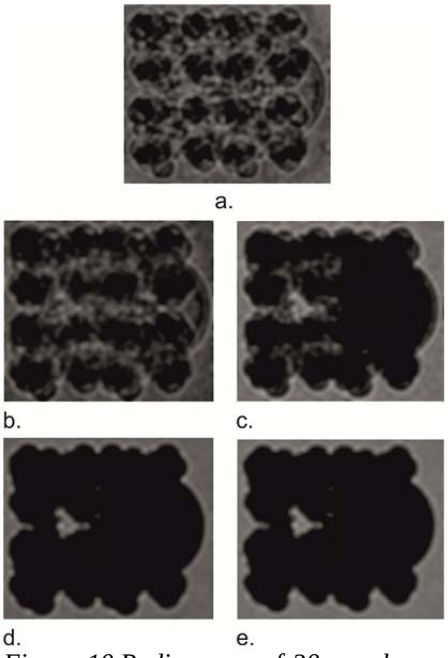

Figure 10.Radiograms of 30 μm drops in front of a core drop, for various values of μ_m.

Summary and Conclusions

This paper has presented the results of a simulation for x-ray radiography in sprays. It is a companion piece to an article analyzing x-ray phase contrast imaging. Here we have shown that radiography detects the total liquid mass along a line of sight, including both drops and intact liquid (when vapor and gas absorption are negligible). As such, it reveals liquid mass fraction which is related to the spray breakup rate and gas entrainment; both critical for understanding of sprays. This work has identified a potential for confusion between darkening by diffraction and darkening by absorption. The problem is actually not unusual in such circumstances. This potential background problem can be avoided by careful arrangement of the experiment and it is clear that it does not affect the results produced by the Advanced Photon Source.

Acknowledgements

The author is grateful to Dr. William Bachalo of Artium Technologies Inc. for very helpful and enlightening discussions. He is also grateful to Dr. George Lawrence of Applied Optics Research for very useful and insightful advice on the application of GLAD to this problem.

References

1. Blessing, M., et al. *SAE Technical Paper no. 2003-01-1358: Analysis of Flow and Cavitation Phenomena in Diesel Injection Nozzles and its Effects on Spray and Mixture Formation*. 2003.
2. Linne, M.A., et al., *Ballistic Imaging of Liquid Breakup Processes in Dense Sprays.* Proceedings of the Combustion Institute, 2009. **32**: p. 2147-2161.
3. Sedarsky, D., et al., *Fast-framing ballistic imaging of velocity in an aerated spray.* Optics Letters, 2009. **34**(18): p. 2748-2750.
4. MacPhee, A.G., et al., *X-ray imaging of shock waves generated by high-pressure fuel sprays.* Science, 2002. **295**: p. 1261-1263.
5. Cai, W., et al., *Quantitative analysis of highly transient fuel sprays by time-resolved x-radiography.* Applied Physics Letters, 2003. **83**(8): p. 1671-1673.
6. Renzi, M.J., et al., *Pixel array detectors for time resolved radiography.* Review of Scientific Instruments, 2002. **773**(3): p. 1621-1624.
7. EL-Hannouny, E.M., et al. *SAE Technical Paper Series, paper no. 2003-01-3150: Near-Nozzle Spray Characteristics of Heavy-Duty Diesel Injectors*. 2003.
8. Tanner, F.X., et al., *Structure of high-velocity dense sprays in the near-nozzle region.* Atomization and Sprays, 2006. **16**: p. 579–597.
9. Kastengren, A.L., et al. *SAE Technical Paper Series, paper no. 2007-01-0666: Determination of Diesel Spray Axial Velocity Using X-Ray Radiography*. 2007.
10. Kastengren, A.L., et al., *Measurement of Biodiesel Blend and Conventional Diesel Spray Structure Using X-Ray Radiography.* Journal of Engineering for Gas Turbines and Power, 2009. **131**.
11. Kastengren, A., et al. *SAE Technical Paper Series, paper no. 2011-01-0383: Correlation of Split-Injection Needle Lift and Spray Structure*. 2011.
12. Gao, J., et al., *Morphology of Diesel Sprays from Single-Orifice Micronozzles*, in *ILASS-Americas*. 2010: Cincinnati, OH.
13. Linne, M., *Detailed Numerical Analysis of X-ray Phase Contrast Imaging in Sprays*, in *ICLASS - 12th International Conference on Liquid Atomization and Spray Systems*. 2012: Heidelberg, DE.
14. Wang, J., *X-ray Vision of Fuel Sprays.* Journal of Synchrotron Radiation, 2005. **12**: p. 197-207.
15. Malave-Sanabria, A., *Diesel Sprays Imaging Using X-rays*, in *Mechanical Engineering*. 2007, University of Wisconsin-Madison: Madison, WI.

16. Linne, M., *Analysis of X-Ray Radiography in Atomizing Spray*. Experiments in Fluids, 2012.
17. Robert, E., et al., *Table-top flash X-ray diagnostics of dodecane sprays*, in *ILASS-Europe*. 2010: Brno, CZ.
18. Balewski, B., *Experimental investigation of the influence of nozzle-flow properties on the primary spray breakup*, in *Mechanical Engineering*. 2009, Technical University of Darmstadt: Darmstadt, Germany.
19. Kastengren, A.L., et al., *Spray Diagnostics at the Advanced Photon Source 7-BM Beamline*, in *ILASS-Americas*. 2010: Cincinnati, OH.
20. Linne, M., *Spectroscopic Measurement: An Introduction to the Fundamentals*. 2002, London, UK.
21. Lawrence, G.N., *GLAD Theory Manual, Ver. 5.5*. 2009.
22. Linne, M., *Analysis of X-ray phase contrast imaging in atomizing sprays.* Experiments in Fluids, 2012. **15**(5): p. 1201-1218.
23. Lin, K.C., et al., *Ultrafast X-Ray Study of Aerated-Liquid Jets in a Quiescent Environment*, in *ILASS-Americas*. 2008: Orlando, FL.
24. Powell, C.F., et al. *SAE Technical Paper Series, paper no. 2001-01-0531: X-Ray Measurements of High Pressure Diesel Sprays*. 2001.
25. Kastengren, A.L., et al., *Axial Development of Diesel Sprays at Varying Ambient Density*, in *ILASS-Americas*. 2010: Cincinatti, OH.
26. Lin, K.-C., et al., *Mapping of 3-D Liquid Mass Distribution Within Aerated-Liquid Jets Using X-Ray Radiography* in *ILASS-Americas*. 2012: San Antonio.